The crystal structure of the Ca^{2+}-ATPase 1 from *Listeria monocytogenes* reveals a pump primed for dephosphorylation.

Sara Basse Hansen,[1,2] Mateusz Dyla,[1,2] Caroline Neumann,[1,2] Jacob Lauwring Andersen,[1,2§] Magnus Kjaergaard[1-4] and Poul Nissen[1,2,4*]

[1] Department of Molecular Biology and Genetics, Aarhus University

[2] The Danish Research Institute for Translational Neuroscience (DANDRITE)

[3] Aarhus Institute of Advanced Studies (AIAS)

[4] The Danish National Research Foundation Center for Proteins in Memory (PROMEMO)

[*] Corresponding author: pn@mbg.au.dk

§ Present address: Hamlet Protein, Horsens, Denmark

Abstract:

Bacteria regulate intracellular calcium concentrations by exporting calcium from the cell using active transporters. These transporters include homologues of the mammalian sarco/endoplasmic reticulum Ca^{2+}-ATPase (SERCA), which has served as a paradigm for the structure and mechanism of P-type ATPase ion transport. Here we present three crystal structures of the Ca^{2+}-ATPase 1 from *Listeria monocytogenes* (LMCA1). Structures with BeF_3^- mimicking a phosphoenzyme state reveal an intermediate between the outward-open E2P and the proton-occluded E2-P* conformations known for SERCA. This suggests that LMCA1 pre-organizes for dephosphorylation already at the E2P state, consistent with the rapid dephosphorylation of this pump and observations from single-molecule studies. Comparison of ion binding sites show that an arginine side-chain occupies the position equivalent to the calcium binding site I in SERCA leaving a single Ca^{2+}-binding site in LMCA1, corresponding to SERCA site II. Absence of putative proton pathways suggest a direct mechanism of proton counter transport through the Ca^{2+} exchange pathways. In total, the new structures provide insight into the evolutionary divergence and conserved features of an important class of ion transporters.

Introduction

Ca^{2+} regulation is critical for all cells, and therefore also for bacterial cell biology and survival [1]. Active transporters pump Ca^{2+} across the membrane to maintain low intracellular Ca^{2+} concentrations [2]. Mechanistic details of the calcium transport mechanism have been derived mainly for the sarco-endoplasmic reticulum Ca^{2+}-ATPase (SERCA) and are assumed to extrapolate to other calcium pumps. However, Ca^{2+}-ATPases work in a range of different environments across the domains of life, which suggests that transport mechanisms may adapt also to specific conditions. To understand how adaptive mechanisms translate sequence variations among Ca^{2+}-ATPases to specific functions, it would be desirable to obtain detailed structural information of a more diverse pool of Ca^{2+}-ATPases.

The gram-positive bacteria *Listeria monocytogenes* expresses a Ca^{2+}-ATPase (LMCA1), which is homologous to mammalian Ca^{2+}-ATPases. Soil is the natural habitat of *Listeria*, but they can develop into food borne pathogens causing listeriosis through infection of the bloodstream, spinal cord membranes and brain. LMCA1 extrudes Ca^{2+} across the bacterial membrane in exchange for a proton [3]. In contrast to mammalian cells, opportunistic bacteria have to survive in a range of different external environments. LMCA1 thus allows *Listeria* to survive in infected host cells, where Ca^{2+} concentration can reach the millimolar range in phagosomal compartments [4]. Furthermore, LMCA1 is part of a complex regulatory network associated with alkaline pH tolerance in the intracellular compartments [5]. LMCA1 is therefore an important determinant of *Listeria* cell biology and an attractive candidate for a broader insight into Ca^{2+}-ATPase mechanisms.

Ca^{2+}-ATPases comprise the P2A and P2B subtypes of the P-type ATPases, which all share a conserved domain structure and key features of their transport mechanisms via formation and breakdown of a phosphoenzyme intermediate. The closest mammalian homologue of LMCA1 is SERCA with 34-39% sequence identity depending on the isoform, while the secretory pathway Ca^{2+}-ATPases (SPCA) and plasma-membrane Ca^{2+}-ATPases (PMCA) share 34% and 27-30% sequence identity with LMCA1, respectively [3]. The Ca^{2+}-ATPases have a

TM (transmembrane) domain consisting of ten helical segments (M1-10), which are connected to a cytoplasmic headpiece defined by three cytosolic domains: an A (actuator), an N (nucleotide) and a P (phosphorylation) domain (Figure 1D). The configurations of the domains relative to each other relate to different functional states of the reaction cycle, and how they associate to kinetic properties [6].

Although SERCA and LMCA1 share functional and mechanistic properties they are also different. Per molecule of ATP hydrolyzed, SERCA transports 2 Ca^{2+} ions out and counter transports 2-3 protons [7, 8], while LMCA1 only transports a single Ca^{2+} out and most likely one proton in return [3]. Likewise, SPCA and PMCA only transport a single Ca^{2+} across the membrane. The preserved Ca^{2+} site is the SERCA site II, while the SERCA site I is replaced with other functionalities in LMCA1 [3], PMCA- [9], and SPCA-type [10] Ca^{2+}-ATPases. Homology modeling and mutational studies of LMCA1 suggested that an arginine (Arg795) occupies the region corresponding to Ca^{2+} binding site I in SERCA and may account for a high pH optimum in LMCA1 (pH 8.75-9.5) relative to SERCA (pH ~7) [3]. Furthermore, kinetic comparisons suggested that LMCA1 and SERCA have different rate limiting steps [11].

The mechanism of Ca^{2+}-ATPases has been described in detail by crystal structures of SERCA trapped by inhibitors at specific intermediate steps of the transport cycle [12]. Overall, ATP hydrolysis drives large structural rearrangements that alter the pump from an inward open (E1) to an outward open state (E2), thereby moving Ca^{2+} across the membrane. Binding of Ca^{2+} to the E1 state leads to ATP dependent phosphorylation of a catalytic aspartate in the P domain [13, 14] in a compact state (E1P). Following phosphoryl transfer, the A domain makes an overall large rotation in formation of an outward-open E2P state [15], via a Ca^{2+}-occluded E2P state and an ADP release step at intermediate position of the A domain that have not been observed yet in crystal structures. Reverse reactions with ADP and Ca^{2+} binding in the outward-open E2P state are prevented by a low intracellular ADP concentration and tight binding of a conserved TGES loop in the A domain recognizing the phosphorylated P domain. This is crucial for the directionality of the cycle. Negatively charged residues in the ion binding sites in the membrane are protonated and induce closure of TM domain from the outward-open state. This transition is associated with a small

rotation of the A domain that places the glutamate side chain of the TGES loop to activate a water molecule for the dephosphorylation reaction by a nucleophilic attack [16-18]. Dephosphorylation leads to the proton-occluded E2 state stabilized by a hydrophobic cluster that ensures tight association between M2-A and A-M3 linkers and the P domain with a K^+ site [19, 20]. Proton release to the cytoplasmic side allows the pump to explore the inward-open E1 state and Ca^{2+} binding.

Previously, LMCA1 was crystallized in the Ca^{2+}-free dephosphorylation intermediate (here denoted E2-P_i) based on the octahedral coordination of planar AlF_4^- as a mimic of the pentavalent (trigonal bipyramidal) transition state of dephosphorylation. The structure was determined and partially refined at 4.3 Å resolution [21], but did not permit any detailed analysis. We have also investigated LMCA1 using single-molecule FRET (smFRET) [11, 22]. These data indicated that LMCA1 could be paused in E2P states by introduction of a four-glycine insert (G_4) into the A-M1 linker, most noteworthy showing an occluded E2P state preceding Ca^{2+} release.

Here, we present three crystal structures of LMCA1 stabilized by metallofluoride analogs of phosphorylation: a G_4 mutant structure at 3.0 Å resolution with BeF_3^- and wild-type structures at 4.0 Å resolution, a new structure with BeF_3^- and an improved structure with AlF_4^-.

Results

To gain new functional insight we crystallized the G_4 mutant of LMCA1 in the E2-BeF_3^- form and obtained better diffracting crystals. Bound BeF_3^- adopts a tetrahedral geometry when coordinated by the Asp side chain of the phosphorylation site, and it stabilizes a complex mimicking an E2P phosphoenzyme of P-type ATPases. This resulted in a new crystal form with improved diffraction properties and allowed refinement of the structure at 3.0 Å resolution despite of a challenging unit cell comprising 8 molecules in the asymmetric unit related by non-crystallographic symmetry (Figure S1). The refined structure of LMCA1 derived from this crystal form was then used as a molecular replacement model for two data

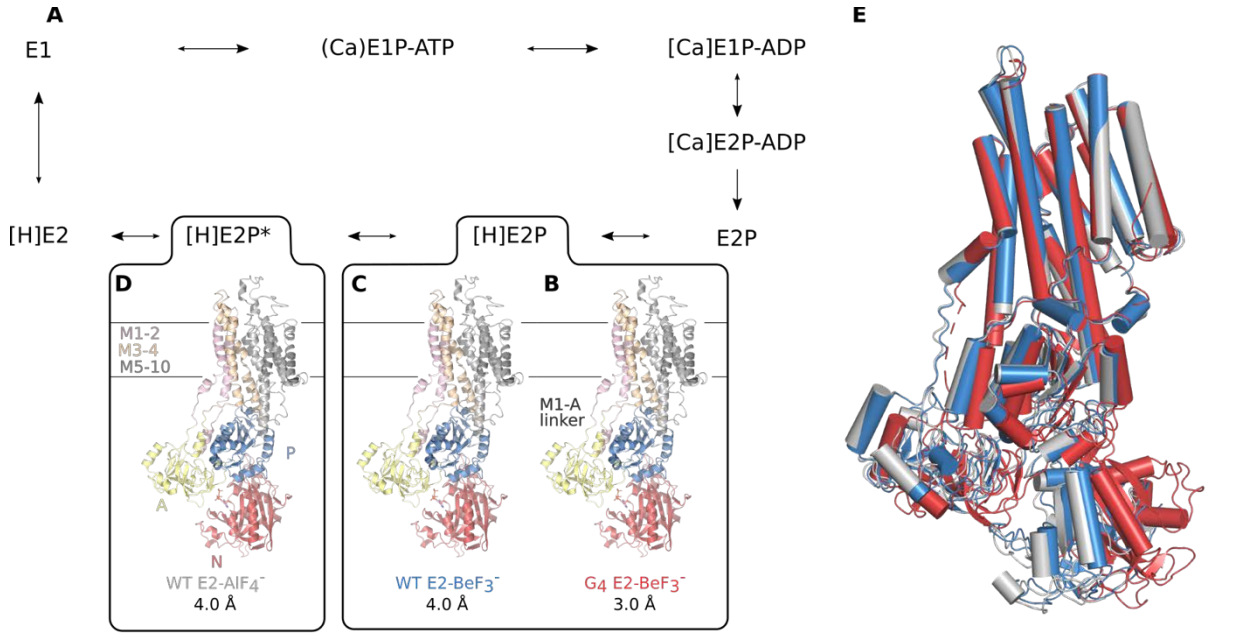

Figure 1 **LMCA1 structures adopt proton-occluded E2 states.** (A) The reaction cycle of LMCA1 with crystal structures represented by (B) G_4 E2-BeF_3^-, (C) WT E2-BeF_3^- and (D) WT E2-AlF_4^-. The structures are colored according to the different domains. (E) An alignment of WT E2-AlF_4^- (light grey), WT E2-BeF_3^- (blue) and G_4 E2-BeF_3^- (red). All the structures are aligned by transmembrane helices M7-10.

sets of wild-type LMCA1 in the E2-BeF_3^- and E2-AlF_4^- forms and resulting in two structures determined at 4.0 Å.

Overall conformation

All three crystal structures show the overall structure expected for a P-type ATPase with three cytoplasmic domains connected to a membrane domain with 10 transmembrane segments (Figure 1B-D). Surprisingly, WT E2-BeF_3^- and WT E2-AlF_4^- adopt the same overall conformation, while in G_4 E2-BeF_3^- the position of the cytosolic domains relative to the TM is altered (Figure 1E). The closed conformation of the cytoplasmic domains suggests that the cytoplasmic domains are trapped in E2-P_i like conformations. Moreover, a closed extracellular pathway suggests that the ion binding site is occluded. A thorough investigation of the ion binding site reveals no indication of Ca^{2+} present at the site, and all three structures

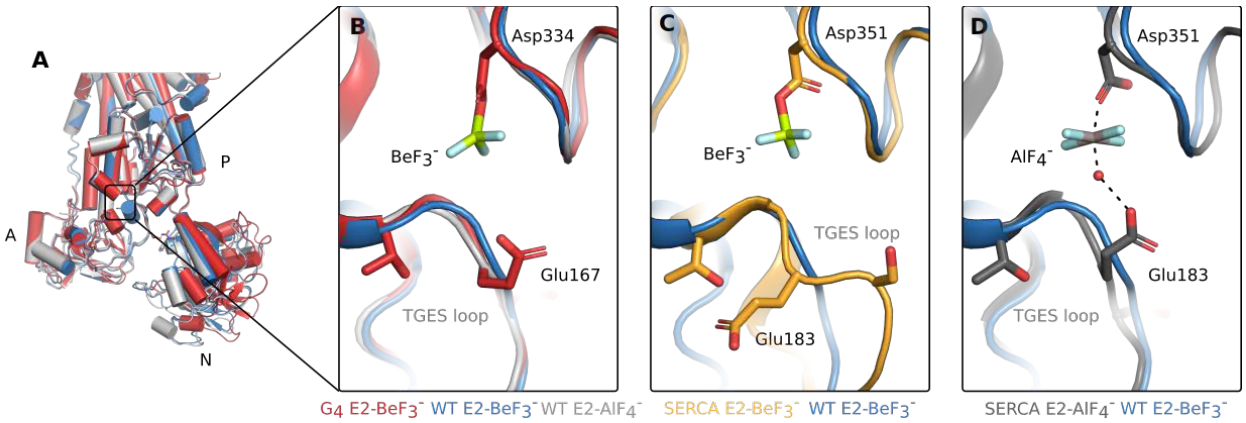

Figure 2 The TGES loop in the E2P state is pre-positioned to catalyze dephosphorylation in LMCA1, but not in SERCA. (A) LMCA1 WT E2-AlF_4^- (light grey), WT E2-BeF_3^- (blue) and G_4 E2-BeF_3^- (red). (B) Zoom of the TGES loop of (A). The TGES loop of LMCA1 WT E2-BeF_3^- aligned with (C) SERCA E2-BeF_3^- (pdb: 3b9b) (orange) and (D) SERCA E2-AlF_4^- (pdb: 3b9r) (dark grey). All the structures are aligned by the P domain.

appear to represent proton-occluded states (Figure 1B-D). In the following, we will focus on the structure with the highest resolution (G_4 E2-BeF_3^-) when discussing detailed structural features.

The structures stabilized by BeF_3^- and AlF_4^- inform on extracellular Ca^{2+} release and protonation coupled to dephosphorylation. For the WT E2-BeF_3^- and E2-AlF_4^- structures, the N domain is poorly defined in the electron density maps. The asymmetric unit of the G_4 E2-BeF_3^- crystal contains eight copies of the protein, where four have N domains that are well-defined in electron density, while the other four exhibit weak density for the N domains (Figure S2). Weak density indicates flexibility, which can be due to the absence of nucleotide in the structures and a minimal role of the N-domain in dephosphorylation. Crystal packing can also affect domain-domain stabilization.

Moreover, the M1-A linker region of the G_4 mutant appears to be flexible, which uncouples the A domain and the position of the entire cytoplasmic headpiece relative to the TM-domain (Figure 1E). The relative position of the N domain of the G_4 E2-BeF_3^- structure differs from that of the WT structure, but the P and A domains maintain the same relative configuration (Figure 2A), only tilted relative to the TM domain.

Interaction between the TGES loop in the A domain and the P domain

The A-P domain interface is critical for dephosphorylation, which is coupled to protonation and occlusion of the extracellular ion exchange pathway. Besides the TGES loop interacting with the phosphorylation site, the interface is also stabilized by Asp186 of the A-domain forming an ionic interaction with Arg598 of the P-domain. Only the G_4 E2-BeF_3^- structure allows proper refinement of side chain orientations, but similarity of local backbone conformations of the available LMCA1 structures hint at generally preserved interactions in all three structures. In SERCA, the A-P domain interface is connected by several ionic bonds referred to as an 'electrostatic catch' centered on Arg198 in the A domain, which is also important for the dephosphorylation rate of SERCA [23]. This residue is not conserved in LMCA1, which indicates that LMCA1 dephosphorylation is not dictated by a similar interaction. Despite the fewer interactions defining the A-P domain interface in LMCA1, smFRET experiments have shown that the pump dephosphorylates rapidly and indicate that the required interactions form quickly [11]. This suggests that with fewer interactions involved, a catalytically competent state is reached faster in LMCA1.

The two metallo-fluorides used as phosphate analogues trap LMCA1 in states before and during dephosphorylation. In all three structures, the A domain is fully rotated and associated with the P domain in a position that corresponds to the dephosphorylation state of SERCA (E2-P_i) (Figure 2A). In G_4 E2-BeF_3^- the TGES loop orients the side chain of Glu167 (Glu183 in SERCA) towards the phosphate analogue, i.e. poised for dephosphorylation (Figure 2B). In SERCA, the calcium-free, BeF_3^--complex adopts an outward-open E2P state, where the TGES loop shields the phosphorylated aspartate and the Glu183 side chain (corresponding to LMCA1 E167) points away from the phosphorylation site (Figure 2C). SERCA only adopts an occluded, dephosphorylation state in the AlF_4^--complex, where Glu183 approaches the phosphorylation site and activates the water molecule that acts as the nucleophile in the hydrolysis (Figure 2D). Since LMCA1 E2-BeF_3^- and E2-AlF_4^- complexes have similar domain arrangements as SERCA E2-AlF4-, no large-scale conformational changes seem necessary to initiate the phosphatase activity following Ca^{2+} release (Figure

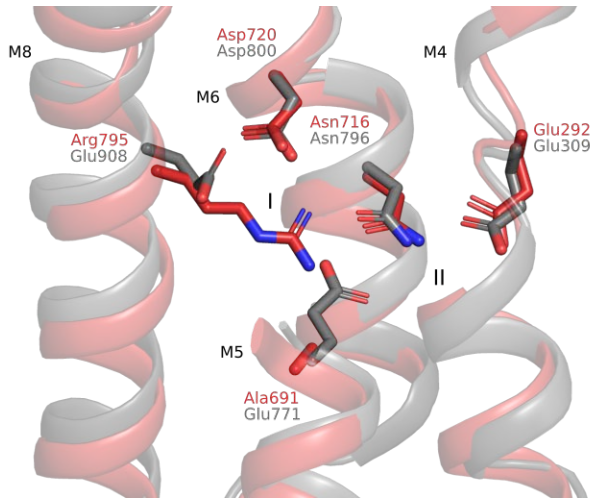

Figure 3 The binding site I of SERCA is not conserved in LMCA1. Alignment between LMCA1 G_4 E2-BeF_3^- (red) and SERCA E2-AlF_4^- (pdb: 3b9r) (dark grey). Relevant Ca^{2+}-coordinating residues are shown as sticks. The structures are aligned by the residues shown as sticks. SERCA Ca^{2+} binding site I and II are indicated.

2B). It suggests that LMCA1 adopts a state preactivated for dephosphorylation upon Ca^{2+} release.

Calcium pathways and binding sites

In LMCA1 the Ca^{2+} release pathway is closed in all structures, sealed with an ionic bond between Asp702 (loop M5-6) and Arg261 (M3) and van der Waal interactions. These residues are not conserved in SERCA. The closed extracellular pathway in LMCA1 is further supported by a hydrophobic cluster consisting of Leu107, Met110, Met163, Leu164, Ile215, Val625 and Val646 that associates M2, M3 and the P domain at the cytoplasmic side; this is conserved in SERCA as a characteristic feature of proton-occluded E2 structures [15, 18, 24].

LMCA1 transports a single Ca^{2+} and counter transports a single proton per hydrolyzed ATP [3]. Alignment of the crystal structures show that the Ca^{2+} binding site of LMCA1 is indeed conserved when compared to site II in SERCA (Figure 3). Arg795 replaces the Ca^{2+}-coordinating Glu908 found in SERCA and occupies the site corresponding to site I (Figure 3) as proposed previously [3]. The other ion coordinating residue of site I in SERCA (Glu771)

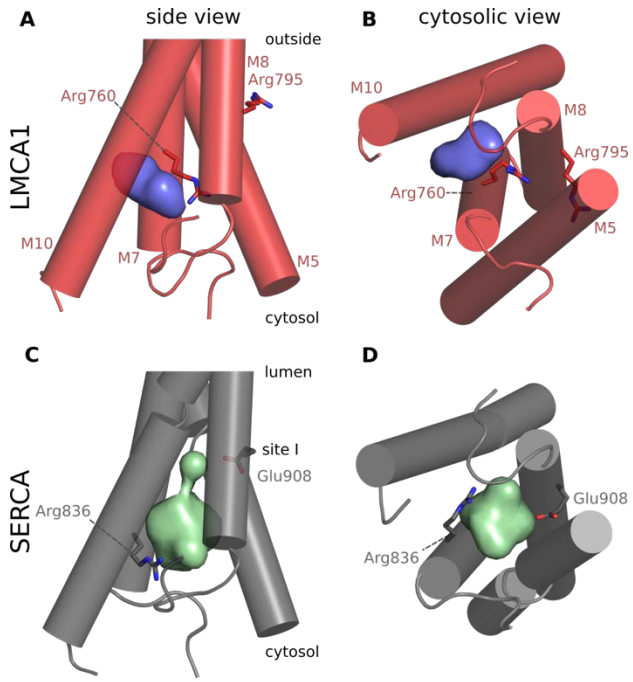

Figure 4. The C-terminal, cytosolic pathway leading to site I in SERCA is absent in LMCA1. (A, B) G_4 E2-BeF_3^- (red), Arg760 blocks the C-terminal pathway. The water cavity (purple) does thus not lead to Arg795. (C, D) In SERCA E2-AlF_4^- (pdb: 3b9r) (dark grey), the C-terminal pathway (green) forms a larger, continuous cavity that leads to the ion binding site I. Only M5, M7, M8 and M10 are shown, and the cytosolic domains are omitted for clarity.

[25] is replaced by Ala691 in LMCA1. The short side chain leaves space for the Arg795 to extend into the core of the LMCA1 TM domain and substitute for Ca^{2+} coordination.

Mechanism of proton counter-transport

SERCA has two proposed proton pathways: a luminal entry pathway [26] and a C-terminal cytosolic release pathway [27]. These are in addition to the luminal Ca^{2+} release pathway between M1/M2, M3/M4 and M5/M6 [15] and the N-terminal cytosolic Ca^{2+} entry pathway between M1, M2, and M3 [13]. The luminal proton pathway has been mapped to a narrow water channel that consists of hydrophilic residues in M5 and M7, leading protons to binding site I [26]. The corresponding part of LMCA1 is mainly hydrophobic, indicating that protons cannot enter through this pathway. The C-terminal cytosolic pathway that is proposed to lead protons from binding site I to the cytosol in SERCA is also different in LMCA1 (Figure 4A,B). In SERCA it consists of a hydrated cavity between M5, M7, M8 and M10 (Figure 4C,D)

[27]. In LMCA1, small hydrophobic residues and Arg760 in M7 extend into this cavity. This leaves only a minute cavity in the corresponding area leading to site I in SERCA. M7 in LMCA1 further blocks the pathway leading from this volume, and LMCA1 therefore does not appear to have a C-terminal cytosolic pathway either. It suggests that protonation and deprotonation take place through the same pathways used for Ca^{2+} transport.

Ca^{2+} binding sites in Ca^{2+}-ATPases are also responsible for proton counter-transport by protonation of glutamate and aspartate residues involved in Ca^{2+}-coordination. In SERCA, the two glutamates (Glu908 and Glu771) in site I are assumed to be protonated from the lumen in the Ca^{2+} free states, and shuttle proton across the membrane in the E2-E1 transition [28]. These proton-transporting side chains are not present in LMCA1, so how are protons then counter-transported? Proton counter transport is observed in LMCA1 [3] and low pH stabilizes the E2 states of LMCA1 [11] suggesting that the ion binding site is indeed protonated in the Ca^{2+} free state. Unless at very high resolution, crystal structures do not reveal protonation directly, but the structure of the ion binding site leaves only two potential candidates that can be reversibly protonated: Glu292 and Asp720 (corresponding to Glu309 and Asp800 in SERCA). To determine the protonation state of these residues, we estimated pK_a values based on the G_4 E2-BeF_3^- crystal structure using PROPKA [29]. The pK_a values of Glu292 and Asp720 are estimated at 8.8 and 5.5, respectively, which suggests that Asp720 remains negatively charged in the E2P state, whereas Glu292 is protonated and therefore likely responsible for proton counter-transport in LMCA1. The corresponding residue in SERCA, Glu309, interacts with the cytosol through the Ca^{2+} entry pathway in the E1 state [27], and it is also exposed directly to the Ca^{2+} release pathways in E2P states. Assuming a similar switch of orientation in LMCA1 makes Glu292 a good candidate site for uptake and transport of a proton in LMCA1. The proton will be taken up from a luminal pathway that closes again quickly in pre-activation of dephosphorylation upon Ca^{2+} release. This may explain why no distinct proton pathways are required in LMCA1.

Discussion

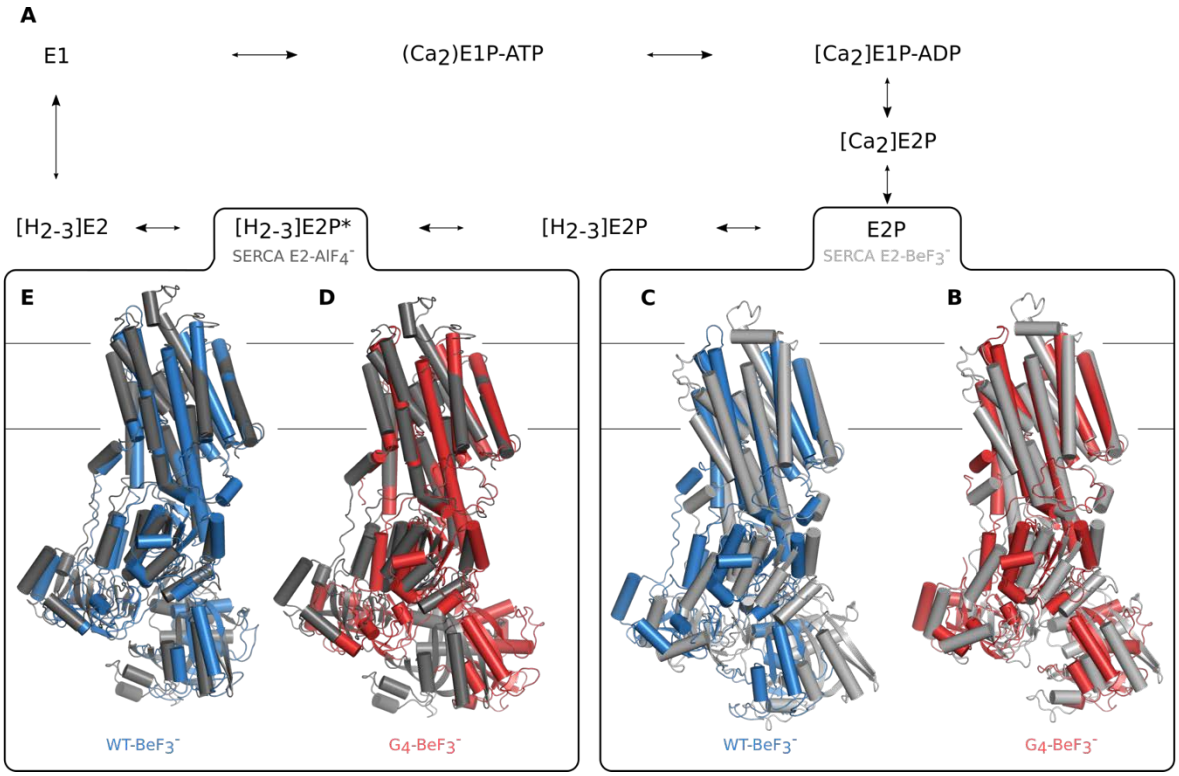

Figure 5. Comparison of SERCA and LMCA1. (A) The reaction cycle of SERCA with crystal structures represented as (B-C) SERCA-BeF_3^- (pdb: 3b9b) (light grey) and (D-E) SERCA-AlF_4^- (pdb: 3b9r) (dark grey). The LMCA1 WT-BeF_3^- form (blue) has a headpiece orientation more similar to the SERCA E2-AlF_4^- form, whereas the LMCA1 G4-BeF_3^- (red) form have an orientation more similar to SERCA E2-BeF_3^-. The structures are aligned by transmembrane helices M7-10.

We have determined and refined three crystal structures of LMCA1 in E2-BeF_3^- and E2-AlF_4^- bound forms representing the E2P and E2-P_i transition state of dephosphorylation. In all cases the TGES loop is pre-positioned for dephosphorylation and the TM domain is occluded. The structures reveal the architecture of the single Ca^{2+} binding site of LMCA1 and suggest a different mechanisms of proton counter-transport compared to SERCA. The structural comparison suggests that core mechanisms of the active Ca^{2+} binding site is conserved across a billion years of divergent evolution, but also that LMCA1 and SERCA are individually fine-tuned for different physiological environments. Insertion of four glycine in the linker between the A domain and M1 of LMCA1 causes the enzyme to pause in a Ca^{2+}-occluded E2P state [11, 30]. The BeF_3^- stabilized form of this mutant showed no bound Ca^{2+} and represents a proton-occluded pre-state of dephosphorylation, similar to structures of the wild-type enzyme with BeF_3^- and AlF_4^-, although with slightly altered angle of the cytoplasmic domains

relative to the TM domain. This change in angle may be an underlying cause of the delayed E1P to E2P transition.

Interdomain interactions account for the fast rate of dephosphorylation

A smFRET study showed that relative rates of partial reactions differ between LMCA1 [11] and SERCA [23]. LMCA1 is rate limited by phosphorylation, dephosphorylates rapidly, and thus predominantly accumulates in E1 states during steady-state pumping [11]. But which structural differences between SERCA and LMCA1 account for the different dephosphorylation rates? Crystal structures of E2-BeF_3^- and E2-AlF_4^- complexes show that LMCA1 and SERCA adopt different conformations when stabilized by the same phosphate analogues. SERCA E2-BeF_3^- forms an outward-open E2P state with the TGES loop shielding the phosphate analogue. However, the LMCA1 E2-BeF_3^- and E2-AlF_4^- complexes adopt a similar conformation to SERCA E2-AlF_4^- and represent a proton-occluded intermediate state of dephosphorylation. The LMCA1 structures all have the TGES loop in a position, where the glutamate side chain can orient a water molecule for in-line attack on the phosphorylated aspartate of the P domain (Figure 5A,C). An outward-open E2P state and a proton-occluded E2-P_i intermediate state are likely in rapid equilibrium, but the structural studies suggest differences in the relative energy of these states between LMCA1 and SERCA - SERCA may change its conformation to induce dephosphorylation in response to uptake of 2-3 protons through separate pathways to an outward-open E2P state stabilized by many interactions, whereas protonation, occlusion and activation of the dephosphorylation site is favored in LMCA1 directly upon Ca^{2+} release.

Binding sites for one or two Ca^{2+}

While SERCA transports two Ca^{2+} per cycle, other mammalian P-type ATPases such as a PMCA and SPCA transport only a single Ca^{2+} like LMCA1. A decreased transport stoichiometry increases the driving force for ion transport, but removes regulatory mechanisms of cooperative binding as in SERCA, and likely it represents adaptation to different physiological roles. Recently, a low resolution cryo-EM structure of PMCA was determined [9], which allows further comparison between the single Ca^{2+} binding site of

mammalian and bacterial Ca^{2+}-ATPases. Similar to LMCA1, PMCA has an active ion binding site that corresponds to site II in SERCA. In LMCA1, the missing calcium binding site I is filled with a positive charge from an arginine residue at a position corresponding to Glu908 in SERCA; a trait that is shared among a range of bacterial Ca^{2+}-ATPases [3]. In PMCA, the corresponding position is occupied by a neutral glutamine [9], while the residue corresponding to Glu771 in SERCA is an alanine for PMCA. No structure has been reported for the SPCA family, but the ion binding site composition can be predicted from homology modeling [31]**.** No compensating positive charge is found in SPCA, but an aspartic acid occupies the position of the Arg795 in LMCA1, and it may be a unique protonation site. Instead, the calcium site I of SPCA is rendered unfunctional by an alanine in the position of SERCA Glu771 like for LMCA1 and PMCA. This shows that Ca^{2+}-ATPases have evolved different mechanisms to alter the transport stoichiometry, and the charge replacement strategy found in LMCA1 is not the only strategy for stabilizing a non-functional ion binding site.

Mechanism of proton counter-transport

The altered ion binding site in LMCA1 suggests an altered mechanism of proton counter-transport. Our crystal structures indicate that Glu292 (Glu309 in Ca^{2+} site II of SERCA) has an elevated pK_a, which is the functional requirement for a protonation site at physiological or even alkaline pH. In SERCA, Glu309 is both protonated and deprotonated from the cytosolic side of the membrane [27], and is thus not believed to counter-transport protons. For Glu292 in LMCA1 to participate in counter-transport, the protonation must occur from the extra-cellular side. SERCA has two luminal ion pathways, which suggests that the protons enter through the luminal proton pathway, while Ca^{2+} is released through the main ion pathway. This has been hypothesized to allow rapid neutralization of the empty binding site, which would otherwise be unstable due to the high negative charge [32]. Furthermore, protonation of Glu309 is believed to be crucial to closure of the luminal pathway and transition to the proton-occluded state mimicked by SERCA E2-AlF_4^- [15]. LMCA1 does not seem to have such an additional proton pathway, and protonation must occur directly through the ion exit pathway. This direct mechanism may relate to the fact that only a single

site is involved. This has resemblance to the P3-type H^+-ATPases that also seem to feature single entry and exit pathways [33, 34]. In a variable external environment, an outward-open state is potentially vulnerable to spurious interactions with compounds. Rapid occlusion and dephosphorylation may also be an evolutionary mechanism of protection in outward-facing pumps.

The proton-occluded E2P state precedes dephosphorylation

A molecular dynamics study of SERCA proposed that after Ca^{2+} release, the pump transits into a proton-occluded E2P state with a closed luminal pathway before dephosphorylation [17]. A key prediction of this study was the formation of an intermediate between known crystal structures [17]. This predicted intermediate would correspond to the occluded structure stabilized by BeF_3^- that is observed here, and the direct observations of such an intermediate from LMCA1 crystal structures is consistent with these simulations. Such an intermediate may have been observed earlier in the crystal structure of SERCA in an E2-BeF_3^- form with the inhibitor thapsigargin [35]. This structure also has a proton-occluded TM domain and cytoplasmic domains in the E2P state with the phosphorylation site shielded by the TGES loop. The LMCA1 structures determined here are more similar to the thapsigargin bound SERCA and especially in the orientation of the TM1-2 helices.

M1-A linker couples the cytosolic domains and TM

The structure of G_4 E2-BeF_3^- aligns well to WT E2-BeF_3^- (Figure 1D) and SERCA E2-AlF_4^- in the TM domain as a proton-occluded state (Figure 5B), but the cytosolic domains are different. The arrangement of the cytosolic domains in G_4 E2-BeF_3^- complex are more reminiscent of SERCA E2-BeF_3^- than WT E2-BeF_3^- (Figure 5). We noted two different clusters of conformations in the 8 copies of the asymmetric unit (Figure S1A), where the orientation of the cytoplasmic domains varies slightly relative to the TM domain (Figure S1B). This suggests that the entire cytosolic headpiece is subject to rigid body movements, and that extension of the A-M1 linker alters the interdomain dynamics.

In SERCA, the G_4-insertion in the A-M1 linker extends the lifetime of a $[Ca_2]$E2-BeF_3^- intermediate state preceding Ca^{2+} release [30], and this state can be entered both through a forward and a reverse reaction. In LMCA1, smFRET data also showed that the G_4 mutant stabilized, albeit only briefly, the Ca^{2+}-occluded E2P state under pumping conditions. We crystallized the LMCA1 G_4 mutant form in the E2-BeF_3^- form in the presence of Ca^{2+}, but observed no bound Ca^{2+}. The smFRET study of LMCA1 offers a rationale for this as Ca^{2+} and ADP release was observed to be practically irreversible for LMCA1 [11]. Thus, despite of the presence of high concentrations of Ca^{2+}, LMCA1 apparently cannot enter this Ca^{2+}-occluded E2P intermediate in the reverse direction, and the G_4 thus crystallize in a Ca^{2+}-free form. Unlike the WT complexes, we did not observe density for the central part of the G_4-extended A-M1 linker in the crystal structure of G_4 E2-BeF_3^-, showing that indeed it gains flexibility and probably overrides mechano-chemical coupling.

Conclusion

We reported structures of a prokaryotic Ca^{2+}-ATPase, which allowed us to shed light on both the reaction cycle and the evolutionary diversification of P-type ATPases. We observed an intermediate that was predicted by molecular dynamics simulations, which suggests that multiple intermediates are involved. Since SERCA has been the model for Ca^{2+}-ATPases, it will be particularly interesting to see how well its properties extrapolate to transporters with a single site Ca^{2+}-ATPases. The smFRET studies previously hinted at a meta-stable Ca^{2+}-occluded E2 form, which still awaits structural characterization. Integration of time-resolved methods with atomic structures are key to illuminating their functional importance. The crystal structures reported here will inform future smFRET studies as they inform the choice of fluorophore labelling sites and development of alternative structural viewpoint for time-resolved studies. Ca^{2+}-ATPases are ubiquitous through-out all domains of life. With these structures of prokaryotic Ca^{2+}-ATPases, we illuminate how ATPases diverge mechanistically and structurally through-out evolution. One can only wonder what remains in store for us.

Materials and Methods

Mutagenesis

G_4-LMCA1 (G_4): Four glycines between residue K44 and D45 in LMCA1-pET-22b were introduced using the QuickChange mutagenesis kit (Agilent Technologies) and verified by Sanger sequencing (Eurofins, MWG).

Expression and purification

LMCA1-pET-22b or G_4-LMCA1-pET-22b, containing a ten-histidine tag and a Tobacco Etch Virus (TEV) protease site in the C-terminus was expressed and purified according to the protocol described in [3]. The solubilized membranes were either pre-packed HisTrap HP column (GE Healthcare) or incubated with 1 ml Ni^{2+} slurry (Ni-sepharose 6 Fast Flow, GE Healthcare) per 1 L expression medium for 1 hour and packed into a XK-16 column (GE Healthcare). The protein was eluted with 150 mM imidazole in buffer C (50 mM Tris-HCl, 200 mM KCl, 20% v/v glycerol, 1 mM $MgCl_2$, 5 mM β-mercaptoethanol (BME), 0.25 mg/ml octaethylene glycol monododecyl ether ($C_{12}E_8$), pH = 7.6). TEV (1 mg per 20 mg protein) digested the eluted LMCA1 while dialyzed against buffer C without imidazole (1:100). The flow-through from a gravity flow Ni^{2+} column was collected and concentrated to ~10 mg/mL using Vivaspin (MWCO = 50 kDa), followed by size-exclusion chromotography (SEC) on a Superdex 200 Increase 10/300 GL column (GE healthcare) equilibrated in 100 mM MOPS, 80 mM KCl, 20% v/v glycerol, 3 mM $MgCl_2$, 5 mM BME, 0.25 mg/ml $C_{12}E_8$, pH = 6.8. Finally, the collected LMCA1 was concentrated to ~10 mg/mL.

Relipidation, crystallization and data collection

G_4 E2-BeF_3^-: In order to relipidate LMCA1, the protocol for the HiLiDe approach [16] was followed. A 5 mL glass tube were rinsed with a flow of gas N_2 to remove the O_2. 0.3 mg 1,2-dioleoyl-*sn*-glycero-3phosphatidylcholine (DOPC) solubilized in $CHCl_3$ was added to the glass tube, and the $CHCl_3$ was evaporated with N_2. Subsequently, 100 μL G_4 E2-LMCA1 were added, the tube was sealed with parafilm and stirred at 50 rpm using microstirring bars at 4° overnight. Insoluble material was removed by centrifugation at 190.000 x g for 10 minutes, and the supernatant was supplemented with 2 mM $CaCl_2$ and a premix of 0.1 mM $BeSO_4$ and 0.5 mM NaF. 1 μL of the protein solution was mixed with 1 μL of reservoir solution (18% PEG2000, 8% glycerol, 8% MPD, 100 mM $MgCl_2$ and 50 mM Tris with pH = 7.2) on a

cover slip and equilibrated against 500 μL of the reservoir solution using hanging drop vapor diffusion method. It was sealed with immersion oil (Merck) and equilibrated at 19 °C. Crystals were mounted in loops from mother liquid and flash frozen in liquid N_2. A complete data set was collected on the P13 beamline at PETRA III radiation source of Deutches Elektronen-Synchrotron (DESY) using a PILATUS 6 M detector.

WT E2-BeF_3^- was relipidated using the same approach as for G_4 E2-BeF_3^-. 0.3 mg DOPC and 0.75 mg $C_{12}E_8$ solubilized in H_2O were added to 100 μL G_4. After centrifugation, LMCA1 was treated with 2 mM ethylene glycol-bis(β-aminoethyl ether)-*N*,*N*,*N*′,*N*′-tetraacetic acid (EGTA) and 1 mM $BeSO_4$ premixed with 5 mM NaF. 1 μL of protein solution was mixed with 1 μL of modified reservoir solution (7% PEG6000, 3% t-BuOH, 100 mM $LiSO_4$, 5 mM BME, 100 mM KCl, 19 mM C_8E_4) on a cover slip and equilibrated against 500 μL of reservoir solution (10% PEG6000, 10% glycerol, 3% t-BuOH, 100 mM $LiSO_4$, 5 mM BME) using hanging drop vapor diffusion method. It was sealed with immersion oil (Merck) and equilibrated at 19°C. Crystals were mounted in loops from mother liquid and flash frozen in liquid N_2. The expression, purification, relipidation, crystallization and data collection of WT E2-AlF_4^- was described in [21].

Homology models

Homology models were made using an online version of Modeller [36] provided by the Bioinformatics Toolkit from Max-Planck Institute for Developmental Biology. A sequence alignment of LMCA1 and SERCA performed in MUSCLE [37] was used as an input file together with the PDB structures of 3B9B and 3B9R for SERCA stabilized with BeF_3^- and AlF_4^-, respectively.

Structure determination

Reflections were indexed and integrated with *XDS* [38] and scaled with *Aimless* [39]. The structure of G_4 E2-BeF_3^- was performed by molecular replacement by *Phaser* [40] using a hybrid search model consisting of WT E2-AlF_4^- [21] with the N domain of LMCA1 homology model of rabbit SERCA-BeF_3^- (PDB: 3B9B) [15]. The structure determination was

challenging, since pseudo-symmetry was present (Figure S1). G_4 E2-BeF_3^- seemed to display orthorhombic symmetry, since the β angle was close to 90° and the self-rotation function at kappa 180° showed three symmetry axes parallel to the crystallographic axes. However, the processing statistics clearly indicated that orthorhombic symmetry was not correct. The space group is the monoclinic $P2_1$, which only exhibits two-fold symmetry. The self-rotation function at kappa 180° reveals the presence of rotational pseudosymmetry parallel to the crystallographic symmetry axis. A native Patterson function [41] analysis revealed a peak with a 29% height relative to the origin, which indicates the presence of translational pseudosymmetry. The non-crystallographic symmetry (NCS) operators close to true crystallographic symmetry operators made molecular replacement challenging, but was eventually solved revealing an unusually packing of eight molecules in the asymmetric unit (Figure S1A). NCS averaging was used during refinement and the data was refined at 3 Å (Table S1). The higher resolution of G_4 E2-BeF_3^- provided a better model for solving and improving structure refinement with lower resolution data sets.

WT E2-BeF_3^- and E2-AlF4- crystals both exhibit $P2_12_12$ symmetry, The structure of WT E2-BeF_3^- was solved by molecular replacement using G_4 E2-BeF_3^- as the search model in *Phaser* [40] and refined at 4.0 Å. For the WT E2-AlF_4^- structure, earlier obtained diffraction images [21] were reprocessed in *XDS* [38] and scaled with *Aimless* [39]. Molecular replacement in *Phaser* [40] solved the structure using WT E2-BeF_3^- as a search model. Refinement of all of the structures was made in *PHENIX* [42] and model building and analyses were performed in *Coot* [43]. Cavities are calculated in HOLLOW [44].

References:

1. Dominguez, D.C., M. Guragain, and M. Patrauchan, *Calcium binding proteins and calcium signaling in prokaryotes.* Cell Calcium, 2015. **57**(3): p. 151-65.
2. Dominguez, D.C., *Calcium signalling in bacteria.* Mol Microbiol, 2004. **54**(2): p. 291-7.
3. Faxen, K., et al., *Characterization of a Listeria monocytogenes Ca(2+) pump: a SERCA-type ATPase with only one Ca(2+)-binding site.* J Biol Chem, 2011. **286**(2): p. 1609-17.
4. Rosch, J.W., et al., *Calcium efflux is essential for bacterial survival in the eukaryotic host.* Mol Microbiol, 2008. **70**(2): p. 435-44.
5. Giotis, E.S., et al., *Genomic and proteomic analysis of the Alkali-Tolerance Response (AlTR) in Listeria monocytogenes 10403S.* BMC Microbiol, 2008. **8**: p. 102.

6. Dyla, M., et al., *Structural dynamics of P-type ATPase ion pumps.* Biochem Soc Trans, 2019. **47**(5): p. 1247-1257.
7. Levy, D., et al., *Evidence for proton countertransport by the sarcoplasmic reticulum Ca2(+)-ATPase during calcium transport in reconstituted proteoliposomes with low ionic permeability.* J Biol Chem, 1990. **265**(32): p. 19524-34.
8. Cornelius, F. and J.V. Moller, *Electrogenic pump current of sarcoplasmic reticulum Ca(2+)-ATPase reconstituted at high lipid/protein ratio.* FEBS Lett, 1991. **284**(1): p. 46-50.
9. Gong, D., et al., *Structure of the human plasma membrane Ca(2+)-ATPase 1 in complex with its obligatory subunit neuroplastin.* Nat Commun, 2018. **9**(1): p. 3623.
10. Dode, L., et al., *Functional comparison between secretory pathway Ca2+/Mn2+-ATPase (SPCA) 1 and sarcoplasmic reticulum Ca2+-ATPase (SERCA) 1 isoforms by steady-state and transient kinetic analyses.* J Biol Chem, 2005. **280**(47): p. 39124-34.
11. Dyla, M., et al., *Dynamics of P-type ATPase transport revealed by single-molecule FRET.* Nature, 2017. **551**(7680): p. 346-351.
12. Dyla, M., et al., *Structure and Mechanism of P-Type ATPase Ion Pumps.* Annu Rev Biochem, 2019.
13. Winther, A.M., et al., *The sarcolipin-bound calcium pump stabilizes calcium sites exposed to the cytoplasm.* Nature, 2013. **495**(7440): p. 265-9.
14. Sorensen, T.L., J.V. Moller, and P. Nissen, *Phosphoryl transfer and calcium ion occlusion in the calcium pump.* Science, 2004. **304**(5677): p. 1672-5.
15. Olesen, C., et al., *The structural basis of calcium transport by the calcium pump.* Nature, 2007. **450**(7172): p. 1036-42.
16. Gourdon, P., et al., *HiLiDe-Systematic Approach to Membrane Protein Crystallization in Lipid and Detergent.* Crystal Growth & Design, 2011. **11**(6): p. 2098-2106.
17. Das, A., et al., *Conformational Transitions and Alternating-Access Mechanism in the Sarcoplasmic Reticulum Calcium Pump.* J Mol Biol, 2017. **429**(5): p. 647-666.
18. Toyoshima, C., H. Nomura, and T. Tsuda, *Lumenal gating mechanism revealed in calcium pump crystal structures with phosphate analogues.* Nature, 2004. **432**(7015): p. 361-8.
19. Sorensen, T.L., et al., *Localization of a K+ -binding site involved in dephosphorylation of the sarcoplasmic reticulum Ca2+ -ATPase.* J Biol Chem, 2004. **279**(45): p. 46355-8.
20. Olesen, C., et al., *Dephosphorylation of the calcium pump coupled to counterion occlusion.* Science, 2004. **306**(5705): p. 2251-5.
21. Andersen, J.L., et al., *Crystallization and preliminary structural analysis of the Listeria monocytogenes Ca(2+)-ATPase LMCA1.* Acta Crystallogr Sect F Struct Biol Cryst Commun, 2011. **67**(Pt 6): p. 718-22.
22. Dyla, M., et al., *Engineering a Prototypic P-type ATPase Listeria monocytogenes Ca2+-ATPase 1 for Single-Molecule FRET Studies.* Bioconjug Chem, 2016.
23. Daiho, T., et al., *Mutations of Arg198 in sarcoplasmic reticulum Ca2+-ATPase cause inhibition of hydrolysis of the phosphoenzyme intermediate formed from inorganic phosphate.* FEBS Lett, 1999. **444**(1): p. 54-8.
24. Yamasaki, K., et al., *Assembly of a Tyr122 Hydrophobic Cluster in Sarcoplasmic Reticulum Ca2+-ATPase Synchronizes Ca2+ Affinity Reduction and Release with Phosphoenzyme Isomerization.* J Biol Chem, 2015. **290**(46): p. 27868-79.

25. Toyoshima, C., et al., *Crystal structure of the calcium pump of sarcoplasmic reticulum at 2.6 A resolution.* Nature, 2000. **405**(6787): p. 647-55.
26. Karjalainen, E.L., K. Hauser, and A. Barth, *Proton paths in the sarcoplasmic reticulum Ca(2+) -ATPase.* Biochim Biophys Acta, 2007. **1767**(11): p. 1310-8.
27. Bublitz, M., et al., *Ion pathways in the sarcoplasmic reticulum Ca2+-ATPase.* J Biol Chem, 2013. **288**(15): p. 10759-65.
28. Rui, H., et al., *Proton Countertransport and Coupled Gating in the Sarcoplasmic Reticulum Calcium Pump.* J Mol Biol, 2018. **430**(24): p. 5050-5065.
29. Dolinsky, T.J., et al., *PDB2PQR: an automated pipeline for the setup of Poisson-Boltzmann electrostatics calculations.* Nucleic Acids Res, 2004. **32**(Web Server issue): p. W665-7.
30. Daiho, T., et al., *Stable structural analog of Ca2+-ATPase ADP-insensitive phosphoenzyme with occluded Ca2+ formed by elongation of A-domain/M1'-linker and beryllium fluoride binding.* J Biol Chem, 2010. **285**(32): p. 24538-47.
31. Vangheluwe, P., et al., *Intracellular Ca2+- and Mn2+-transport ATPases.* Chem Rev, 2009. **109**(10): p. 4733-59.
32. Musgaard, M., L. Thogersen, and B. Schiott, *Protonation states of important acidic residues in the central Ca(2)(+) ion binding sites of the Ca(2)(+)-ATPase: a molecular modeling study.* Biochemistry, 2011. **50**(51): p. 11109-20.
33. Pedersen, B.P., et al., *Crystal structure of the plasma membrane proton pump.* Nature, 2007. **450**(7172): p. 1111-4.
34. Focht, D., et al., *Improved Model of Proton Pump Crystal Structure Obtained by Interactive Molecular Dynamics Flexible Fitting Expands the Mechanistic Model for Proton Translocation in P-Type ATPases.* Front Physiol, 2017. **8**: p. 202.
35. Toyoshima, C., et al., *How processing of aspartylphosphate is coupled to lumenal gating of the ion pathway in the calcium pump.* Proc Natl Acad Sci U S A, 2007. **104**(50): p. 19831-6.
36. Sali, A. and T.L. Blundell, *Comparative protein modelling by satisfaction of spatial restraints.* J Mol Biol, 1993. **234**(3): p. 779-815.
37. Edgar, R.C., *MUSCLE: multiple sequence alignment with high accuracy and high throughput.* Nucleic Acids Res, 2004. **32**(5): p. 1792-7.
38. Kabsch, W., *Xds.* Acta Crystallogr D Biol Crystallogr, 2010. **66**(Pt 2): p. 125-32.
39. Evans, P.R. and G.N. Murshudov, *How good are my data and what is the resolution?* Acta Crystallographica Section D-Biological Crystallography, 2013. **69**: p. 1204-1214.
40. McCoy, A.J., et al., *Phaser crystallographic software.* J Appl Crystallogr, 2007. **40**(Pt 4): p. 658-674.
41. Patterson, A.L., *A direct method for the determination of the components of interatomic distances in crystals.* Zeitschrift Fur Kristallographie, 1935. **90**(6): p. 517-542.
42. Afonine, P.V., R.W. Grosse-Kunstleve, and P.D. Adams, *A robust bulk-solvent correction and anisotropic scaling procedure.* Acta Crystallogr D Biol Crystallogr, 2005. **61**(Pt 7): p. 850-5.
43. Emsley, P. and K. Cowtan, *Coot: model-building tools for molecular graphics.* Acta Crystallogr D Biol Crystallogr, 2004. **60**(Pt 12 Pt 1): p. 2126-32.
44. Ho, B.K. and F. Gruswitz, *HOLLOW: generating accurate representations of channel and interior surfaces in molecular structures.* BMC Struct Biol, 2008. **8**: p. 49.